Laccase biosensors based on different enzyme immobilization strategies for phenolic compounds determination

E. Casero [a], M.D. Petit-Domínguez [a], L. Vázquez [b], I. Ramírez-Asperilla [a], A.M. Parra-Alfambra [a], F. Pariente [a], E. Lorenzo [a,*]

[a] Departamento de Química Analítica y Análisis Instrumental, Facultad de Ciencias, Universidad Autónoma de Madrid (UAM), Campus Internacional de Excelencia UAM+CSIC, c/Francisco Tomás y Valiente No. 7, 28049 Madrid, Spain
[b] Instituto de Ciencia de Materiales de Madrid (CSIC), Campus de Excelencia UAM+CSIC, c/Sor Juana Inés de la Cruz No. 3, 28049 Madrid, Spain

ABSTRACT

Different enzyme immobilization approaches of Trametes versicolor laccase (TvL) onto gold surfaces and their influence on the performance of the final bioanalytical platforms are described. The laccase immobilization methods include: (i) direct adsorption onto gold electrodes (TvL/Au), (ii) covalent attachment to a gold surface modified with a bifunctional reagent, 3,3'-Dithiodipropionic acid di (N-succinimidyl ester) (DTSP), and (iii) integration of the enzyme into a sol–gel 3D polymeric network derived from (3-mercaptopropyl)-trimethoxysilane (MPTS) previously formed onto a gold surface (TvL/MPTS/Au). The characterization and applicability of these biosensors are described. Characterization is performed in aqueous acetate buffer solutions using atomic force microscopy (AFM), providing valuable information concerning morphological data at the nanoscale level.

The response of the three biosensing platforms developed, TvL/Au, TvL/DTSP/Au and TvL/MPTS/Au, is evaluated in the presence of hydroquinone (HQ), used as a phenolic enzymatic substrate. All systems exhibit a clear electrocatalytic activity and HQ can be amperometrically determined at −0.10 V versus Ag/AgCl. However, the performance of biosensors – evaluated in terms of sensitivity, detection limit, linear response range, reproducibility and stability – depends clearly on the enzyme immobilization strategy, which allows establishing its influence on the enzyme catalytic activity.

© 2013 Elsevier B.V. All rights reserved.

1. Introduction

Nowadays, in nutritional literature, a high effort is devoted to study several aspects of free radicals, a type of unstable compounds produced during metabolic processes. An excess of free radicals in the human body, which can be caused by pollution, sunlight or smoke of cigarettes overexposure, promotes oxidative damage in cells, accelerating the aging process. Among the different compounds with antioxidant properties, polyphenols play a protective role against human diseases associated with oxidative stress. They are commonly present in fruits, legumes, vegetables and several beverages. Accordingly, during the last years, numerous studies aimed at evaluating the antioxidant capacity of natural products, such as wines, teas and herbal infusions, have been reported. In particular, special attention has been paid to the development of new methodologies, such as amperometric biosensors based on tyrosinase, peroxidase or laccase enzymes, which can be employed as alternative methods for total polyphenolic content determination in foods [1–10].

Laccases, which have been employed in a less extent than tyrosinases in the development of amperometric biosensors for phenols quantification, are a type of copper-containing oxidoreductases produced by numerous plants, fungi, and bacteria. In particular, Trametes versicolor laccase, TvL, (dimensions of 7.0 nm × 5.0 nm × 5.6 nm) [11] is a fungal laccase containing four copper ions located in sites denoted as T1, T2 and T3 in the active center of the enzyme [12–14]. Among laccases from different sources, there are remarkable differences such as molecular weight, substrate specificity and optimum pH, but they have in common the capability to oxidize benzenediols/phenols to the corresponding phenones with the concomitant reduction of oxygen. Thus, the detection of polyphenolic compounds can be based on measuring the reduction current of quinones generated as products of the enzymatic reaction.

The performance of enzyme-based amperometric biosensors depends on several factors, mainly on the catalytic activity preservation after the enzyme immobilization onto solid electrodes. Since the immobilization process can produce an alteration of the three-dimensional conformation of the enzyme that leads to a diminution of the catalytic activity, an adequate choice of the immobilization strategy plays a crucial role in the biosensor design and performance. Thus, the development of amperometric biosensors based on

* Corresponding author.
E-mail address: encarnacion.lorenzo@uam.es (E. Lorenzo).

enzyme immobilization onto electrode surfaces in such way that they retain their fully activity and stability has become one of the most important issues in several fields ranging from environmental analysis to clinical diagnosis. In the particular case of laccase-based biosensors, an extensive research effort has been addressed to immobilize laccase on surfaces by different immobilization strategies in order to design biosensors with a wide range of applications [15,16]. In this sense, laccase immobilization has been performed in the literature on different solid supports (glassy carbon, carbon paste, platinum, and gold) using immobilization strategies such as direct adsorption, covalent binding, entrapment in polymeric membranes or gels and cross-linking procedures. Recent advances in this field are related to the development of new support matrix as suitable platforms (most of them including nanomaterials) for enzymes immobilization, which lead to biosensors with improved analytical properties. So, in recent works, laccase has been immobilized onto: epoxy resin membranes [9], mesoporous materials with well-controlled pore structures [10,17], multi-walled carbon nanotubes paste electrodes [18], nanocomposites formed by chitosan and carbon nanotubes [19], copper-containing ordered mesoporous carbon chitosan matrix [8], pyrenehexanoic acid-modified hierarchical carbon microfibers/carbon nanotubes composite electrodes [16], polyvinyl alcohol photopolymers [20], sol–gel matrix of diglycerylsilane [21], 3-mercaptopropionic acid self-assembled monolayer modified gold electrodes [22], cysteine self-assembled monolayer and quantum dots modified gold electrodes [23], nanocomposites of silver nanoparticles and zinc oxide nanoparticles electrochemically deposited onto gold electrodes [24], platinum nanoparticles and reduced graphene composites deposited onto screen printed electrodes [25], polyethyleneimine coated gold-nanoparticles modified glassy carbon electrodes [26], multiwalled carbon nanotubes and polypyrrole electrocodeposited onto platinum electrodes [27]. However, the design of stable and sensitive laccase biosensors in an easy and rapid way is still a great deal of interest, due to their wide range of applications in different fields.

In this paper, we describe the development and characterization of three different laccase, from *Trametes versicolor* (TvL), based biosensors for polyphenols determination. Among the different available strategies to achieve the enzyme immobilization onto gold surfaces, we have focused our attention on: (i) direct adsorption of TvL onto a gold substrate, (ii) covalent bonding to a self-assembled monolayer (SAM) and (iii) encapsulation into a sol–gel matrix. The morphological characteristics at the nanometer level of the developed biosensors were obtained by atomic force microscopy (AFM) technique. The influence of the enzyme immobilization strategy on the analytical performance of the resulting biosensors was evaluated using hydroquinone as a model phenolic substrate.

2. Experimental section

2.1. Reagents and solutions

Laccase (EC 1.1.3.4) from *Trametes versicolor* (TvL), lyophilized powder containing 27.9 U/mg solid, was obtained from the Sigma Chemical Co. (St. Louis, MO). Stock enzyme solution was prepared dissolving 35.7 mg of the TvL lyophilized powder in 250 μL of 0.1 M acetic/acetate buffer solution pH 4.5, aliquoted (10 μL) and stored at −30 °C. Under these conditions, the enzymatic activity remains stable for several weeks. Hydroquinone (HQ), 3,3'-Dithiodipropionic acid di (N-succinimidyl ester) (DTSP), dimethyl-sulfoxide (DMSO) and (3-mercaptopropyl)-trimethoxysilane (MPTS) were also purchased from Sigma Chemical Co. and used as received. Stock solutions of HQ (1 mM) were freshly prepared. Other chemicals used in this work, such as methanol, hydrochloric acid and sodium acetate were used as

received without additional purification steps. Sodium acetate was employed for the preparation of acetic/acetate buffer solutions (0.1 M, pH 4.5) Water was purified with a Millipore Milli-Q-System. All solutions were prepared just prior to use.

2.2. Experimental techniques

2.2.1. Atomic force microscopy measurements

Supports employed for laccase immobilization in AFM measurements consist of glass substrates (1.1 × 1.1 cm^2) covered with a chromium layer (1–4 nm thick) on which a gold layer (200–300 nm thick) was deposited (Metallhandel Schröer GmbH, Lienen, Germany). The AFM measurements were performed with a Nanoscope IIIa equipment (Bruker) operating in intermittent contact and under buffer conditions. Sharp silicon nitride levers (Bruker) with a nominal force constant close to 0.32 N/m were employed. These cantilevers have a silicon tip with a nominal tip radius of about 2 nm. Imaging soft matter under liquid environment with this sharp tip requires an extreme care to keep low the applied tip load since if this is not the case the soft sample feature could be pierced or deformed by the tip. Accordingly, extreme low free amplitudes (around 0.2–0.3 V) were employed. The images were obtained in 3–6 min and were composed by 512 × 512 pixels. The thickness of the MPTS layer was estimated in air conditions with silicon cantilevers through force curve analysis.

2.2.2. Electrochemical measurements

Cyclic voltammetric and amperometric studies were carried out with an Ecochemie Autolab PGSTAT12 system (Utrecht, The Netherlands). The electrochemical experiments were carried out in a three-compartment electrochemical cell with standard taper joints so that all compartments could be hermetically sealed with Teflon adapters. A gold electrode was used as working electrode. A large-area coiled platinum wire was employed as a counter electrode. All potentials were reported against a Ag/AgCl reference electrode without taking into account the liquid junction.

2.3. Procedures

#### 2.3.1. Preparation of the electrochemical biosensing platforms

Prior to each experiment, gold electrodes were polished with 1 μm diamond paste (Buehler) and rinsed with water.

The TvL/Au electrochemical biosensing platform was developed by placing 5 μL of the stock enzyme solution onto the electrode surface. After air-drying, the modified electrodes were washed with water to remove any weakly bound material.

The TvL/DTSP/Au was developed by immersing a gold substrate for 3 h at room temperature in a solution of DTSP (1.0 mM in DMSO). The corresponding monolayer containing the active succinimidyl esters was rinsed in DMSO and water. Subsequently, 5 μl of TvL stock solution was placed onto the modified surface (DTSP/Au) leading to a covalent binding between the enzyme and the succinimidyl esters. After air-drying, the biosensor was washed with water to remove any weakly bound enzyme.

Finally, the development of the TvL/MPTS/Au biosensing platform requires the previous formation of a sol–gel network. In a first step, the sol–gel solution was prepared mixing 200 μL of MPTS with 600 μL of water, 600 μL of methanol and 200 μL of 0.1 M HCl. This solution was sonicated using an Ultrasons bath (P-Selecta) for 30 min at room temperature. Subsequently, the solution was stored for 3 h at room temperature. Afterwards, the gold surface was immersed in the MPTS sol–gel solution, prepared as described above, for 1 h. MPTS sol chemisorbs on the polycrystalline Au electrode forming a 3D silicate network. The resulting MPTS sol-modified electrode was thoroughly rinsed with water to remove
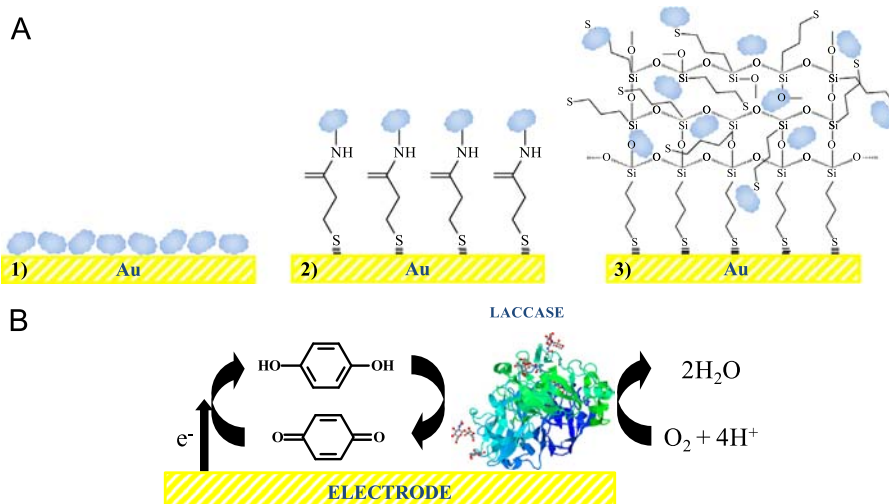
Scheme 1. (A) Enzyme immobilization strategies employed for biosensor fabrication: (1) direct adsorption, (2) covalent binding, and (3) sol–gel encapsulation. (B) Catalytic reaction for phenolic compounds.

the physically adsorbed MPTS sol and finally 5 μL of the TvL stock solution were dropped on this surface. After air-drying, the biosensor was washed with water to remove any weakly bound enzyme.

The three different enzyme immobilization approaches employed for biosensors preparation are summarized in Scheme 1A.

2.3.2. AFM measurements

Gold supports employed for AFM measurements were previously annealed for 2 min in a gas flame in order to obtain Au (111) terraces and imaged in buffer solution to assess that the surface was flat and clean prior to enzyme immobilization. The images, before and after TvL immobilization, were taken with different cantilevers in order to ensure that the imaged structures were not due to tip artefacts.

3. Results and discussion

3.1. Immobilization of TvL onto gold surfaces by different approaches: characterization by AFM.

A critical step in developing biosensors is the enzyme immobilization onto the transducer. Physical adsorption is a rapid and easy way to immobilize enzymes on gold, which is a rather interesting material for bioelectronic devices. However, it may result in low stability of the enzyme on the electrode; thus a stronger linkage is sometimes required for biosensor applications. One of the approaches employed successfully to achieve strong immobilization of enzymes on gold surfaces consists of chemical modification of the electrode surface for favoring specific interactions with the enzyme molecules. Entrapping enzymes into polymeric structures or hydrogels allows a higher concentration of enzyme on the electroactive surface, but the background current is increased. In this work, we have developed and compared three different strategies, based on the principles mentioned above, to immobilize *Trametes versicolor* laccase: (i) direct adsorption onto a gold electrode (TvL/Au), (ii) covalent attachment on a previously functionalized gold surface with an adequate self-assembled monolayer (SAM) (TvL/DTSP/Au) and (iii) encapsulation of TvL onto a sol–gel matrix (TvL/MPTS/Au). In the former case (TvL/Au), the interaction responsible of the enzyme immobilization is unspecific adsorption. In contrast, in the second approach we

have used a well-established strategy to bind covalently proteins. This approach is based on the covalent attachment of proteins containing lysine residues, through acylation of free primary or secondary aliphatic groups, to gold surfaces modified with a bifunctional reagent containing succinimide functionalities, in particular, 3,3' Dithiodipropionic acid di (N-succinimidyl ester) (DTSP). Since DTSP adsorbs onto gold surfaces through the disulfide group, the terminal succinimidyl groups are exposed to the solution allowing further covalent immobilization of amine-containing biomolecules, such as laccase from *Trametes versicolor* (TvL/DTSP/Au). Finally, the third approach is based on TvL encapsulation on a sol–gel 3D polymeric network derived from (3-mercaptopropyl)-trimethoxysilane (MPTS) previously formed onto a gold surface. MPTS presents the advantage of forming a 3D polymeric network containing a large number of thiol tail groups distributed throughout its structure that enable its anchoring onto gold surfaces. Moreover, this matrix provides a biocompatible environment that preserves the catalytic activity of TvL after its immobilization and allows the incorporation of a high amount of enzyme, which is expected to improve the sensitivity of the final biosensing device. Since the performance of the developed biosensors is closely related to several factors including the conformation, distribution and morphology of the immobilized enzyme onto the surface, performing an AFM characterization of each system becomes essential.

Fig. 1A shows a 3.5×3.5 μm^2 image of the gold surface after deposition of laccase by direct adsorption. Clearly, the characteristic micro-granular structure of the underlying gold surface is observed. The bright spots observed in the image correspond to laccase aggregates that usually tend to be formed along the steps and the micro-grain boundaries of the gold surface. Characteristic 0.5×0.5 μm^2 images obtained on the surface of a flat micro-grain (Fig. 1B) reveal that the whole surface is covered by a compact layer of globular structures with characteristic lateral sizes in the 5–8 nm range. In a higher resolution image (75×75 nm^2) of this layer (inset of Fig. 1A) the globular morphology and size of these structures are better observed. As these structures were not present in the as-prepared gold surface (data not shown), and their lateral dimensions are consistent with those of the laccase molecule, we can identify them as those of the laccase deposit. In fact, the brighter (i.e., higher) spots observed in Fig. 1A and B correspond either to single proteins adsorbed on top of the laccase monolayer (with heights in the 6–7 nm range) or to laccase aggregates displaying larger height values (above 10 nm).
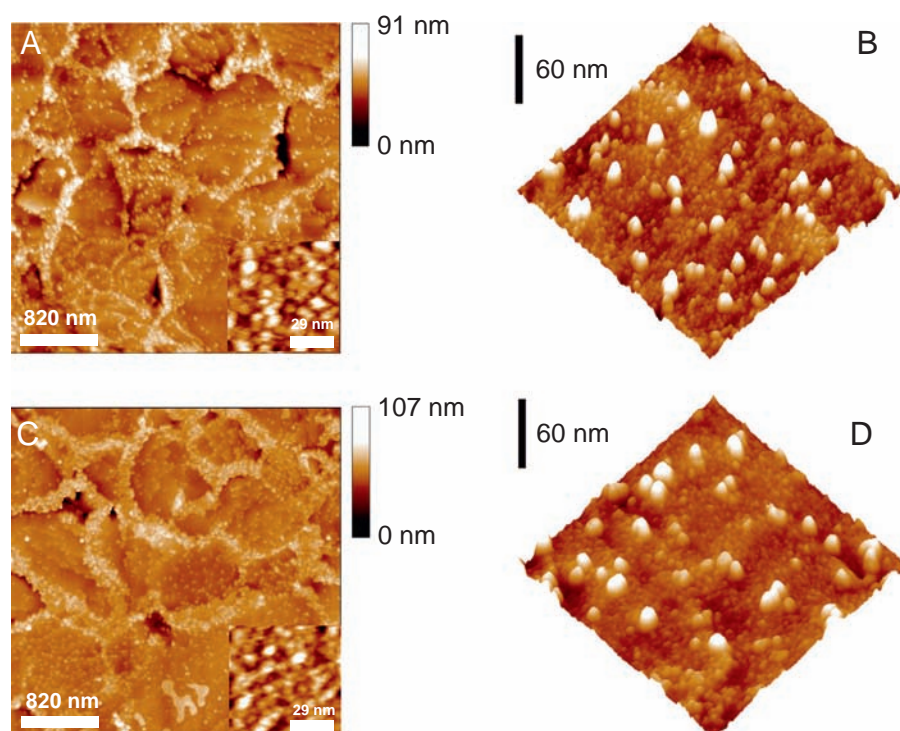
Fig. 1. (A) $3.5 \times 3.5~\mu m^2$ and (B) $0.5 \times 0.5~\mu m^2$ tapping-mode AFM images of a TvL layer adsorbed on a gold substrate. Inset of figure A: a higher magnification image ($75 \times 75~nm^2$) of the same system. (C) $3.5 \times 3.5~\mu m^2$ and (D) $0.5 \times 0.5~\mu m^2$ tapping-mode AFM images of a TvL layer covalently bonded to a DTSP-modified gold substrate. Inset of figure C: a higher magnification image ($75 \times 75~nm^2$) of the same system. All images have been taken under buffer conditions.

The AFM analysis of the TvL/DTSP/Au system (Fig. 1C and D) shows a similar behavior than that observed on the previous system (TvL/Au). Perhaps, the most noticeable difference lies in the fact that it seems that laccase tends to aggregate mainly at the micro-grain boundaries as shown in Fig. 1C. Once more, the images taken on flat micro-grains (Fig. 1D) display a compact laccase monolayer, where the laccase structures show lateral sizes in the 5–7 nm range (see inset of Fig. 1C). Again, some structures 6–8 nm high, are imaged on top of the laccase monolayer, which correspond to laccase structures deposited on top of the under-lying monolayer.

Finally, when laccase is included in a 3D polymeric network, the resulting platform (TvL/MPTS/Au) presents some morphological differences with respect to the two previous ones. In order to better interpret the AFM images obtained in this system, it is convenient to first characterize the MPTS/Au system. Its surface morphology as imaged by AFM is shown in Fig. 2A and B. The larger image (Fig. 2A) shows a flatter surface as the grooves between micro-grains are to some extent blurred or less marked, probably due to the deposit of the polymer layer at these locations. However, some sort of surface roughness is evident in both Fig. 2A and B, although it becomes clear that the MPTS/Au surface morphology at the nano-scale is different from those obtained in laccase-containing systems (compare Fig. 2B with Fig. 1B or D).

The previous data will be useful to interpret those obtained from the AFM images of the TvL/MPTS/Au surface (Fig. 3A and B). In this case, the micro-granular structure of the gold substrate is also blurred or dimmed as the grain boundaries are not so clearly observed now (Fig. 3A). This fact agrees with the observations already reported on the MPTS/Au surface [28]. It is worth to note that the surface of the flat grains is more homogeneous as quite less three dimensional laccase aggregates are imaged (Fig. 3B). However, the high resolution imaging (inset of Fig. 3A) shows that the laccase layer is less compact (more porous) than in the previous cases, where it was physically adsorbed or covalently bonded. This larger porosity together with tip convolution effects, leads to wider globular structures (in the 5–12 nm range) than those previously observed for the other two systems where laccase formed a quite compact monolayer. This fact can be related to the presence of the MPTS layer itself. This soft polymeric layer can swell when immersed in liquid environment as in this case. Under this condition, the sharp tip could pierce this quite soft layer and image laccase structures located at different depths inside the MPTS layer. In this sense, we have tried to estimate the thickness of the MPTS layer. For this purpose, we have taken different force curves in air with the same tip on the Au surface and the MPTS/Au surface.

In Fig. 2C are displayed characteristic force curves taken on the gold surface and at three different spots of the MPTS/Au sample. The steepest slope is observed for the Au sample because of its stiffer character. For the MPTS/Au sample, there is first a curved region, which corresponds to the softer MPTS layer, followed by a straight regime with a slope similar to that measured on Au. This last regime then corresponds to the point where the soft MPTS layer has been pierced and the underlying Au surface has been reached. From the lateral shift at this point between the MPTS/Au curve and that measured on Au, MPTS thickness values ranging from 20 nm up to 75 nm are obtained. Therefore, as one would expect for a 3D network, the MPTS layer could stack a large number of laccase structures at different depths, which would be consistent with the images obtained for the TvL/MPTS/Au system. Based on the above results, it seems clear that the third strategy allows the immobilization of a great number of laccase molecules per unit of geometric area than those based on either direct adsorption or covalent binding to a SAM-modified gold electrode.

3.2. Evaluation of the biosensor response.

Laccase catalyzes the oxidation of benzenediols with concomitant reduction of O_2 to H_2O [29]. In the biosensing platforms
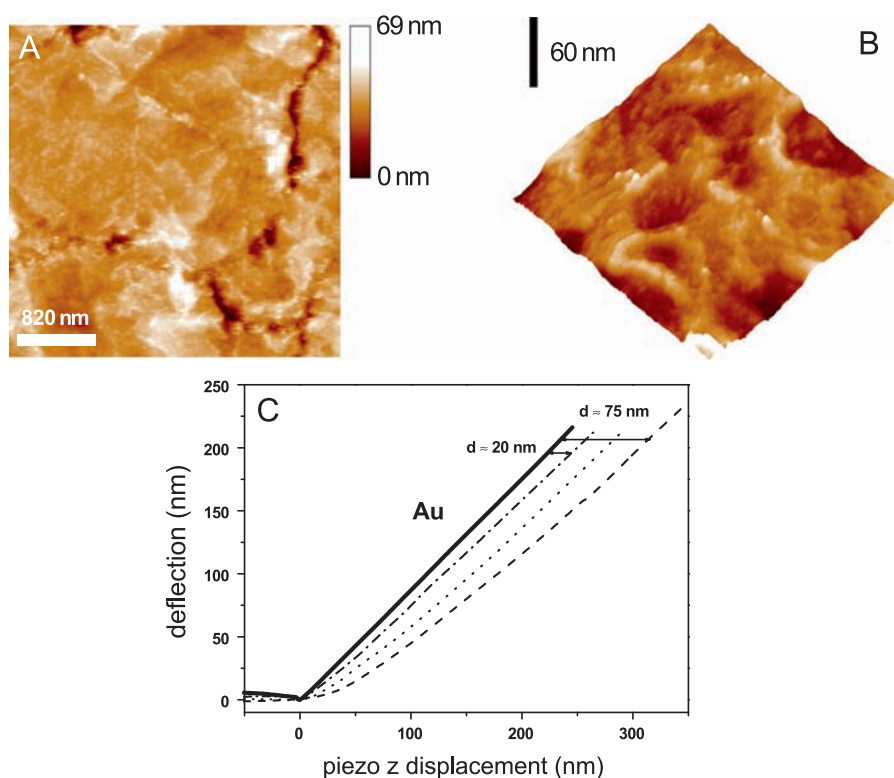
Fig. 2. (A) 3.5 × 3.5 μm² and (B) 0.5 × 0.5 μm² tapping-mode AFM images of MPTS/Au, taken under buffer conditions. (C) Force curves taken in air with the same silicon tip on the gold (solid bold line) and MPTS/Au systems. The curves corresponding to the MPTS/Au (dash-dotted, dotted and dashed lines) have been taken at different sample locations. The thickness of the polymer layer varies in the 20–75 nm range.
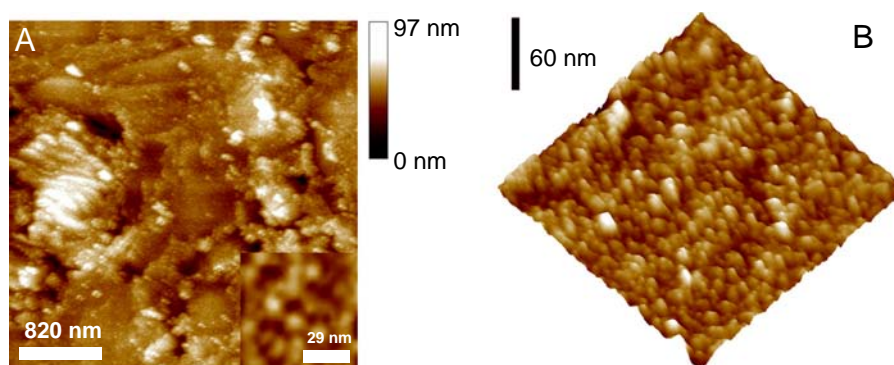
Fig. 3. (A) 3.5 × 3.5 μm² and (B) 0.5 × 0.5 μm² tapping-mode AFM images of TvL/MPTS/Au. Inset of figure A: a higher magnification image (75 × 75 nm²) of the same system. All images have been taken under buffer conditions.

developed in this work, hydroquinone was selected as a model phenolic substrate. According to Scheme 1B, laccase catalyzes the oxidation of hydroquinone to quinone through its active center T1 acting the molecular oxygen as final electron acceptor, which is reduced to water [12]. The quinone enzymatically generated is reduced to hydroquinone at the electrode surface, giving rise to an electrocatalytic current. Thus, the concentration of hydroquinone, or other phenolic substrates, can be determined by monitoring this electrocatalytic current.

In order to assess whether the developed laccase based biosensors present catalytic activity towards phenolic compounds and to evaluate the influence of the enzyme immobilization strategy on the analytical performance of the resulting devices, its cyclic voltammetric response in the absence and in the presence of hydroquinone was obtained.

Hydroquinone presents electrochemical response at gold electrode, thus the first step was to study its response under the same experimental condition than those employed for the biosensor.

Fig. 4A displays the cyclic voltammogram of a bare Au electrode in the presence of hydroquinone in 0.1 M acetate buffer (pH 4.5) solution. As can be observed, when the potential was cycled from +0.18 V (where no faradaic current is observed) towards positive values and then reversed until −0.5 V, a pair of redox peaks with a formal potential of +0.20 V, ascribed to the hydroquinone/quinone redox couple, is observed. The peak potential separation ($\Delta E_p = 400$ mV) is larger than the typical value for two-protons/two-electrons redox reaction, indicating a charge transfer resistance between redox species and electrode surface. If the potential is swept from +0.18 V towards negative values and then reversed until +0.6 V (Fig. 4B), no reduction peak appears in the cathodic scan, indicating the absence of quinones or other oxidants in the initial solution. However, the oxidation of the hydroquinone is evident in the anodic scan.

Fig. 4C shows the cyclic voltammogram response for the TvL/Au biosensing platform in the presence (a) and in the absence (b) of hydroquinone in 0.1 M acetate buffer solution, from −0.5 V to
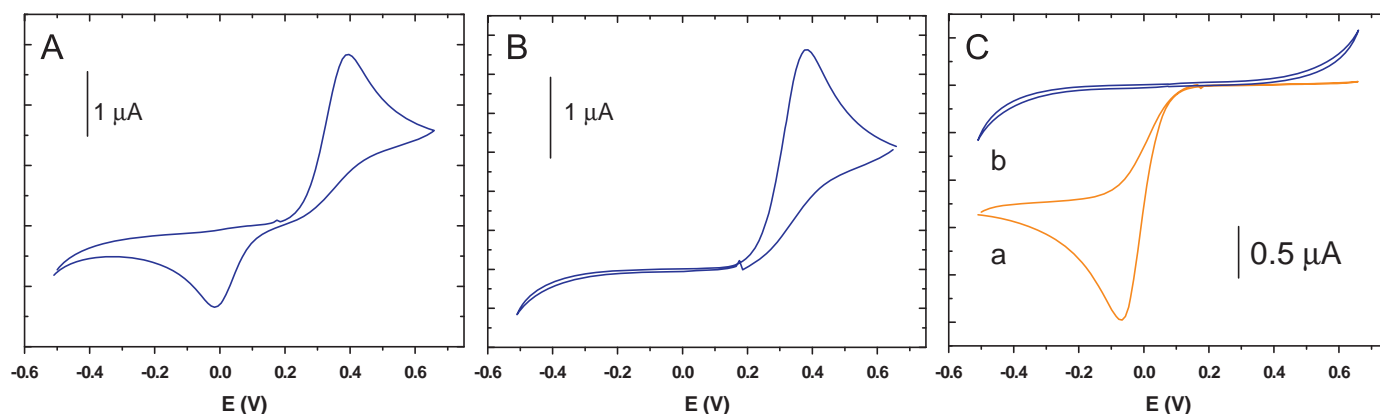
Fig. 4. Cyclic voltammetric response for a bare gold electrode (Au) in 0.1 M acetate buffer (pH 4.5) solution containing 100 μM hydroquinone cycling the potential from +0.18 V towards positive (A) or negative values (B). (C) Cyclic voltammetric response for TvL/Au biosensor immersed in 0.1 M acetate buffer solution (pH 4.5) in the presence (a) and in the absence (b) of 100 μM hydroquinone. The scan rate was 10 mV/s.

+0.65 V at 10 mV/s. The potential sweep was carried out at the same conditions as in Fig. 4B. In the presence of hydroquinone (scan a of Fig. 4C), it can be observed that in the anodic scan there are not oxidation peaks, indicating that hydroquinone was not present near the electrode since the enzymatic reaction was taking place. In contrast, in the cathodic scan, since quinone is generated as product of the enzymatic reaction, a clear response ascribed to its electrocatalytic reduction was observed. Obviously, in the absence of hydroquinone (scan b of Fig. 4C) no peaks were obtained. For both TvL/DTSP/Au and TvL/MPTS/Au platforms, similar cyclic voltammograms to those displayed in Fig. 4C were obtained (Fig. 1S).

The optimal response of biosensors depends on several factors including the degree of catalytic activity preservation after the enzyme immobilization process and operational parameters such as the working pH and the applied potential in chronoamperometric measurements. Concerning operational parameters, we have assayed pH values between 4 and 7 (data not shown). A pH in the 4–5 range was selected since this gives the optimum response, according to the optimum pH value for the enzyme [20]. On the other hand, from Fig. 4C (where the cathodic wave ascribed to the electrocatalytic reduction of p-quinone to hydroquinone appears at −0.07 V) a potential value of −0.10 V was selected to carry out the chronoamperometric experiments, since it is adequate to provide a good intensity signal, minimizing interferences due to other redox compounds. Thus, chronoamperometric measurements of TvL/Au, TvL/DTSP/Au and TvL/MPTS/Au platforms for different HQ concentrations were carried out by posing the biosensor at a step-potential from +0.18 V, where no redox process is occurring, to −0.10 V, where reduction of the quinones generated as products of the enzymatic reaction was assured. From the chronoamperometric response obtained for the developed biosensors in the presence of increasing HQ concentrations (as an example data for TvL/Au system are displayed in Fig. 2S), it can be concluded that a steady state current is reached after 50 s.

Therefore, the current measured at this time was plotted as a function of the concentration of HQ in solution (Fig. 3S) for TvL/Au (curve A), TvL/DTSP/Au (curve B) and TvL/MPTS/Au (curve C) biosensors. The linear concentration range for each biosensor was described by the following linear regression equations: $I_{ss}(\mu A) = 2.29C$ (mM)$+0.0014$ ($R=0.992$) for TvL/Au, $I_{ss}(\mu A) = 2.53C$(mM)$+0.0015$ ($R=0.990$) for TvL/DTSP/Au, and $I_{ss}(\mu A) = 2.84C$(mM)$+0.0048$ ($R=0.990$) for TvL/MPTS/Au. The analytical properties of the developed biosensors, such as linear concentration range, sensitivity, detection limit and reproducibility were evaluated, and are displayed in Table 1. As can be observed, the sensitivity, calculated as the slope of the calibration curves, was 2.29, 2.53, and 2.84 μA m M^{-1} for

TvL/Au, TvL/DTSP/Au, and TvL/MPTS/Au, respectively. Concerning the detection limit, calculated as the ratio between three times the standard deviation of the blank signal and the sensitivity, values of 0.91, 0.89, and 0.25 μM were obtained. As can be concluded from these data, biosensors based on direct adsorption and covalent binding show similar linear concentration ranges that are narrower than the corresponding to sol–gel based one. Regarding sensitivity and detection limit, they are higher and lower respectively, in the case of sol–gel based platforms. These results are consistent with the fact that this approach allows to incorporate a large number of laccase structures at different depths as it was concluded from AFM images. The reproducibility was evaluated from the RSD for five different measurements of 7 μM of hydroquinone, yielding similar values for the biosensors based on the three different immobilization strategies (around 3%).

Thus, if we compare the results obtained for the biosensor based on three dimensional sol–gel network with the results obtained for both dimensional biosensors, based on direct adsorption or covalent binding, we can affirm that the three strategies allowed to prepare very reproducible final biosensing devices. Nevertheless, as one would expect and according to the literature, the three dimensional sol–gel network allows the incorporation of a higher amount of enzyme, which improves the sensitivity of the final biosensing device without lost of reproducibility.

In order to compare the analytical properties obtained for the three developed biosensors with those of other laccase-based biosensors previously described, we have also included in Table 1 data concerning linear concentration range, sensitivity, detection limit and reproducibility of several laccase-based biosensors reported in the literature [3,4,8–10,17,19–21,25–27,30–35]. It is important to highlight that, in general, a direct comparison of the performance of the different biosensors is not straightforward since they employ different detection strategies, they determine different phenolic substrates and they are developed using different sources of enzymes. However, although a high variability of data is observed for each analytical parameter (due to the different nature of biosensors displayed in Table 1), it can be concluded that most of the analytical properties of the biosensors designed by us are comparable or even improved compared to those reported in the literature for other laccase-based biosensors. It is important to highlight that some of the biosensors summarized in the table include nanomaterials, which is not our case. Moreover, an important point to take into account is that related to the simplicity of the biosensor fabrication process. In this sense, the three biosensors designed in the present work involve an easy fabrication process, allowing to obtain similar or better analytical performance than those showed in the table, most of them obtained by more complicated methods.

Table 1
Analytical properties of several laccase-based biosensors reported in the literature, including the present work.

	Substrate	Linear range (μM)	Sensitivity (μA m M^{-1})	Detection limit (μM)	R.S.D.(%)
TvL/Au (present work)	Hydroquinone	3.0–15	2.29 ± 0.11	0.91	2.6 ($n=5$)
TvL/DTSP/Au (present work)	Hydroquinone	3.0–15	2.53 ± 0.14	0.89	3.1 ($n=5$)
TvL/MPTS/Au (present work)	Hydroquinone	0.9–20	2.84 ± 0.16	0.25	3.0 ($n=5$)
Lac/NSTP (from DTSP)/Au [3]	Caffeic acid	2.0–10.0	0.083 ± 0.007	1.3	n.r.
GA/Lac/NSTP (from DTSP)/Au [3]	Caffeic acid	0.1–10.0	33 ± 1	0.072	4.5 ($n=3$)
Lac/Nafion/C [4]	Hydroquinone	0.1–3.0	n.r.	0.035	n.r.
Lac/Cu-OMC-CS/Au [8]	Cathecol	0.67–15.75	104	0.67	2 ($n=6$)
Lac/epoxy/Pt [9]	Guaiacol	0.5–50	n.r.	0.3	n.r.
Lac/FSM7.0/C [10]	Cathecol	2–100	2.63	2.0	8.4 ($n=6$)
MB-MCM-41/PVA/Lac/Au [17]	Cathecol	4.0–87.98	n.r.	0.331	n.r.
Lac/Tyr-CS-MWCNT/ITO [19]	Rosmarinic acid	0.4–6.4	148	0.25	9 ($n=10$)
Lac/Tyr-CS-MWCNT/ITO [19]	Gallic acid	1.6–8.1	33	1.55	16 ($n=10$)
Lac/PVA/C [20]	Hydroquinone	1.1–130	9.44 ± 0.19	1.07	n.r.
Lac-Tyr-sol–gel matrix/Fc/C [21]	Gallic acid	n.r.	0.339 ± 0.008	50	4.9 ($n=5$)
Nafion/Lac/RGO/PtNPs/CSPE [25]	Caffeic acid	0.2–2	2147.38 ± 65.40	0.09	5.7 ($n=7$)
Lac/PEI-AuNPs/C [26]	Hydroquinone	2.90–22.00	1.12 ± 0.006	0.21	6.5 ($n=5$)
Lac/PPy/MWCNT/Pt [27]	Dopamine	0.50–4.75	0.43 ± 0.008	0.14	2.9 ($n=10$)
Lac/C [30]	Hydroquinone	1–10	51	0.58	n.r.
Lac/Nafion/C [31]	Rosmarinic acid	0.7–1.5	n.r.	0.12	1.1 ($n=3$)
Lac/CS-MWCNT/Au [32]	Rosmarinic acid	0.9–12	846	0.23	2.1 ($n=5$)
Nafion/Lac/Sonogel/C [33]	Caffeic acid	0.04–2	99.6	0.06	3.3 ($n=10$)
Lac/C [34]	Hydroquinone	0.5–8	n.r.	0.44	n.r.
Lac/MWCNTs-CS/C [35]	Cathecol	1.2–30	n.r.	0.66	< 7.9 ($n=3$)

n.r.=non-reported, TvL: trametes versicolor laccase; DTSP: 3,3'-dithiodipropionic acid di(N-succinimidyl ester); MPTS: (3-mercaptopropyl)-trimethoxysilane; Au: gold electrode; Lac: laccase; NSTP: N-succinimidyl-3-thiopropionate; GA: glutaraldehyde; C: glassy carbon electrode; OMC: ordered mesoporous carbon; CS: chitosan; Pt: platinum electrode; FSM7.0: mesoporous silica powder; MB: methylene blue; MCM-41: mesoporous silica sieve; PVA: polyvinyl alcohol; Tyr: tyrosinase; MWCNTs: multi-walled carbon nanotubes; ITO: indium tin oxide; Fc: ferrocene; RGO: reduced graphene; PtNPs: platinum nanoparticles; CSPE: carbon screen-printed electrode; PEI: polyethyleneimine; AuNPs: gold nanoparticles; PPy: polypyrrole.

Finally, since the most critical issues for an enzyme immobilization approach are both to avoid the leaking of the immobilized enzyme to the solution and to preserve its catalytic activity, the stability of TvL/Au, TvL/DTSP/Au and TvL/MPTS/Au biosensors was also evaluated by recording successive cyclic voltammograms in 0.1 M acetate buffer (pH 4.5) solution containing 100 μM hydroquinone. From these measurements, displayed in Fig. 1S, it can be concluded that about 89%, 96% and 99% of the initial current response was retained after 50 cycles for TvL/Au, TvL/DTSP/Au and TvLMPTS/Au, respectively. In order to study the storage stability of the three developed biosensors, additional experiments were carried out. Biosensors, stored at 4 °C when not in use, maintain their initial response during the first week of storage, while after 6 weeks TvL/Au, TvL/DTSP/Au and TvL/MPTS/Au retain 87%, 93% and 97% of the initial current response, respectively. These data confirm that the developed biosensing platforms present excellent storage stability, particularly those based on sol–gel technology. This may be due to the biocompatible environment created by the 3D polymeric network.

4. Conclusions

In this paper, the influence of different enzyme immobilization strategies on the performance of TvL biosensing platforms is studied. The three methods selected for the immobilization process are based on different interactions between the enzyme and the surface: (i) unspecific adsorption, (ii) covalent binding and (iii) inclusion in a sol–gel matrix. In presence of a phenolic compound, the biosensing platforms exhibit electrocatalytic activity, and hydroquinone can be amperometrically determined at −0.10 V versus Ag/AgCl. The biosensor based on sol–gel technology exhibits a lower detection limit and a wider linear concentration range, when compared with biosensors based on direct adsorption and covalent binding, respectively. In this sense, this relative biosensing performance enhancement is explained by the incorporation of a higher amount of enzyme, which is enabled by the

three dimensional sol–gel network. In addition, the sol–gel network provides with a biocompatible environment to enzyme encapsulation, leading to biosensors with an excellent stability.

Appendix A. Supporting information

Supplementary data associated with this article can be found in the online version at http://dx.doi.org/10.1016/j.talanta.2013.05.045.

References

[1] S.A.S.S. Gomes, J.M.F. Nogueira, M.J.F. Rebelo, Biosens. Bioelectron. 20 (2004) 1211–1216.
[2] F. Vianello, S. Ragusa, M.T. Cambria, A. Rigo, Biosens. Bioelectron. 21 (2006) 2155–2160.
[3] M.L. Mena, V. Carralero, A. González-Cortés, P. Yáñez-Sedeño, J.M. Pingarrón, Electroanalysis 17 (2005) 2147–2155.
[4] A.I. Yaropolov, S.V. Shleev, O.V. Morozova, E.A. Zaitseva, G. Marko-Varga, J. Emneus, L. Gorton, J. Anal. Chem. 60 (2005) 553–557.
[5] H. Tang, W. Zhang, P. Geng, Q. Wang, L. Jin, Z. Wu, M. Lou, Anal. Chim. Acta 562 (2006) 190–196.
[6] Y. Zhang, G. Zeng, L. Tang, D. Huang, X. Jiang, Y. Chen, Biosens. Bioelectron. 22 (2007) 2121–2126.
[7] Y. Tan, W. Deng, Y. Li, Z. Huang, Y. Meng, Q. Xie, M. Ma, S. Yao, J. Phys. Chem. B 114 (2010) 5016–5024.
[8] X. Xu, M. Guo, P. Lu, R. Wang, Mater. Sci. Eng. C-Mater. 30 (2010) 722–729.
[9] S. Chawla, R. Rawal, R.C. Shabnam, C.S. Kuhad, Anal Pundir, Methods 3 (2011) 709–714.
[10] T. Shimomura, T. Itoh, T. Sumiya, T. Hanaoka, F. Mizukami, M. Ono, Sensor. Actuat. B-Chem. 153 (2011) 361–368.

[11] T. Bertrand, C. Jolivalt, P. Briozzo, E. Caminade, N. Joly, C. Madzak, C. Mougin, Biochemistry 41 (2002) 7325–7333.
[12] S. Shleev, J. Tkac, A. Christenson, T. Ruzgas, A.I. Yaropolov, J.W. Whittaker, L. Gorton, Biosens. Bioelectron. 20 (2005) 2517–2554.
[13] F. Xu, A.E. Palmer, D.S. Yaver, R.M. Berka, G.A. Gambetta, S.H. Brown, E.I. Solomon, J. Biol. Chem. 274 (1999) 12372–12375.
[14] S. Shleev, A. Christenson, V. Serezhenkov, D. Burbaev, A. Yaropolov, L. Gorton, T. Ruzgas, Biochem. J. 385 (2005) 745–754.
[15] N. Durán, M.A. Rosa, A. D'Annibale, L. Gianfreda, Enzyme Microb. Technol. 31 (2002) 907–931.
[16] C. Gutiérrez-Sánchez, W. Jia, Y. Beyl, M. Pita, W. Schuhmann, A.L. De Lacey, L. Stoica, Electrochim. Acta 82 (2012) 218–223.
[17] X. Xu, P. Lu, Y. Zhou, Z. Zhao, M Guo, Mater. Sci. Eng. C-Mater 29 (2009) 2160–2164.
[18] T.M.B.F. Oliveira, M.F. Barroso, S. Morais, P. de Lima-Neto, A.N. Correia, M.B.P.P. Oliveira, C. Delerue-Matos, Talanta 106 (2013) 137–143.
[19] M. Diaconu, S.C. Litescu, G.L. Radu, Microchim. Acta 172 (2011) 177–184.
[20] P. Ibarra-Escutia, J. Juarez-Gómez, C. Calas-Blanchard, J.L. Marty, M.T. Ramírez-Silva, Talanta 81 (2010) 1636–1642.
[21] M.R. Montereali, L.D. Seta, W. Vastarella, R. Pilloton, J. Mol. Catal. B-Enzymatic 64 (2010) 189–194.
[22] F. Vianello, A. Cambria, S. Ragusa, M.T. Cambria, L. Zennaro, A. Rigo, Biosens. Bioelectron. 20 (2004) 315–321.
[23] Z. Wang, Q. Xu, J.H. Wang, Q. Yang, J.H. Yu, Y.D. Zhao, Microchim. Acta 165 (2009) 387–392.
[24] S. Chawla, R. Rawal, D. Kumar, C.S. Pundir, Anal. Biochem. 430 (2012) 16–23.
[25] S.A.V. Eremia, I. Vasilescu, A. Radoi, S.C. Litescu, G.L. Radu, Talanta 110 (2013) 164–170.
[26] D. Brondani, B. de Souza, B.S. Souza, A. Neves, I.C. Vieira, Biosens. Bioelectron. 42 (2013) 242–247.
[27] I. Cesarino, H.V. Galesco, F.C. Moraes, M.R.V. Lanza, S.A.S. Machado, Electroanalysis 25 (2013) 394–400.
[28] A.M. Parra-Alfambra, E. Casero, M.D. Petit-Domínguez, M. Barbadillo, F. Pariente, L. Vázquez, E. Lorenzo, Analyst 136 (2011) 340–347.
[29] A.I. Yaropolov, O.V. Skorobogatko, S.S. Vartanov, S.D. Varfolomeyev, Appl. Biochem. Biotechnol. 49 (1994) 257–280.
[30] A. Jarosz-Wilkolazka, T. Ruzgas, L. Gorton, Talanta 66 (2005) 1219–1224.
[31] S.C. Litescu, S.A.V. Eremia, A. Bertoli, L. Pistelli, G.L. Radu, Anal. Lett. 43 (2010) 1089–1099.
[32] M. Diaconu, S.C. Litescu, G.L. Radu, Sensor. Actuat. B-Chem. 145 (2010) 800–806.
[33] M. ElKaoutit, I. Naranjo-Rodriguez, K.R. Temsamani, M.P. Hernández-Artiga, D. Bellido-Milla, J.L. Hidalgo-Hidalgo de Cisneros, Food Chem. 110 (2008) 1019–1024.
[34] B. Haghighi, L. Gorton, T. Ruzgas, L.J. Jönsson, Anal. Chim. Acta 487 (2003) 3–14.
[35] Y. Liu, X. Qu, H. Guo, H. Chen, B. Liu, S. Dong, Biosens. Bioelectron. 21 (2006) 2195–2201.